Magnetic coupling of stripe domains in FePt/$Ni_{80}Fe_{20}$ bilayers

2017 J. Phys. D: Appl. Phys. 50 115001

(http://iopscience.iop.org/0022-3727/50/11/115001)

IOP Publishing Journal of Physics D: Applied Physics

J. Phys. D: Appl. Phys. **50** (2017) 115001 (10pp) doi:10.1088/1361-6463/aa5bce

Magnetic coupling of stripe domains in FePt/$Ni_{80}Fe_{20}$ bilayers

N R Álvarez[1,2], J E Gómez[1,2], M Vásquez Mansilla[1,2], B Pianciola[1,2], D G Actis[3], G J Gilardi[4], L Leiva[1,5], J Milano[1,2,5] and A Butera[1,2,5,6]

[1] Centro Atómico Bariloche (CNEA), 8400 Bariloche, Río Negro, Argentina
[2] Conicet, 8400 Bariloche, Río Negro, Argentina
[3] Universidad Nacional de La Plata, Buenos Aires, Argentina
[4] Universidad Nacional del Sur, Bahía Blanca, Buenos Aires, Argentina
[5] Instituto Balseiro (U N Cuyo), 8400 Bariloche, Río Negro, Argentina
[6] INN—Instituto de Nanociencia y Nanotecnología, CNEA, Argentina

E-mail: butera@cab.cnea.gov.ar

Received 31 October 2016, revised 13 January 2017
Accepted for publication 24 January 2017
Published 13 February 2017

Abstract

Equiatomic FePt in the A1 soft magnetic phase and $Ni_{80}Fe_{20}$ (permalloy) thin films form a stripe-like magnetic domain structure above a critical thickness. This critical thickness is considerably different in the two alloys and allows us to study the influence of the magnetic coupling in the domain configuration in bilayers. Using dc magnetron sputtering techniques, we fabricated two different sets of FePt/$Ni_{80}Fe_{20}$ bilayers, keeping one thickness fixed and varying the other, and investigated the dc magnetic properties and the magnetic domain configuration of the structure. In all cases, magnetization reversal occurred at a single coercive field, indicating a relatively strong magnetic exchange coupling between both layers. The observed stripe period was also consistent with a model of spring magnet-like behavior. However, for certain values of FePt and permalloy thickness a complex nonparallel double stripe structure was found, which may be attributed to the influence of the dipolar stray field of the thicker layer on the stripe structure of the thinner film.

Keywords: FePt, permalloy, stripe magnetic domains, thin magnetic bilayers, magnetic interactions

(Some figures may appear in colour only in the online journal)

1. Introduction

The magnetic properties of thin films and multilayers in which a magnetic domain structure in the form of stripes has formed have been investigated intensively by different experimental groups [1–10] in the last few decades, and several theoretical models have been proposed to explain the observed behavior [11–16].

Precise control of the formation of stripe domains has implications from a technological point of view, for example for spintronic and magnonic devices [17], exchange spring magnets [18], tunable inductors [19] and microwave antennas [20].

The presence or absence of stripe domains is determined by the competition between different energy terms. Contributions to the magnetic energy, like anisotropy, shape, exchange, the domain wall and the Zeeman effect (for $H \neq 0$), must be taken into account to obtain the minimum-energy configuration. If the anisotropy has a component perpendicular to the film plane (characterized by an anisotropy constant, $K_\perp$), a structure of non-planar domains may be formed, even if the shape anisotropy $2\pi M_s^2$ (M_s is the saturation magnetization) is dominant. When the quality factor $Q = K_\perp/2\pi M_s^2 < 1$, a pattern of mostly parallel stripes defines regions in which a component of the magnetization vector points alternately in opposite out-of-plane directions. The perpendicular anisotropy can have different origins, but is mostly determined by magnetocrystalline, magnetoelastic or interfacial contributions. If $Q < 1$, the formation of a stripe structure only occurs above a critical thickness d_{cr}, which essentially depends on Q and

the exchange stiffness parameter, A. For $Q \sim 0.3$–0.4, the critical thickness is in the range of $d_{cr} \sim 20$–40 nm for Co [2, 21], amorphous Nd–Co [8, 22], epitaxial $Fe_{1-x}Ga_x$ ($x \sim 0.2$) [6], partially ordered FePd [3, 23] or disordered FePt films [5, 24–32]. In films with lower Q, larger values of d_{cr} are generally found, such as in permalloy ($d_{cr} \sim 200$ nm) [33, 34] or Fe–Zr–N ($d_{cr} \sim 450$ nm) [35]. In a very simple approximation the value of the critical thickness is given by twice the classical expression for the domain wall thickness [15], $d_{cr} \sim 2\pi\sqrt{A/K_\perp}$. Samples that obey $Q < 1$ and $d > d_{cr}$ are often called 'transcritical'. The lateral period of the stripe structure at remanence increases with film thickness following a power law [2, 5, 11, 12], $\lambda_s \propto d^x$, with $x \sim 0.5$. There is also a macroscopic coupling between the in-plane and the out-of-plane magnetization components that originates a pseudo-uniaxial in-plane anisotropy, known as rotatable anisotropy [22], which tends to align the in-plane remanent magnetization parallel to the direction of the last applied field (if it is strong enough to reach saturation).

The effects of magnetic interactions on the stripe structure have been studied in different systems. For example, symmetric (Co/Pt)Ru multilayers with strong perpendicular anisotropy can couple ferromagnetically (FM) or antiferromagnetically (AF), depending on the spacer thickness [36, 37]. In both cases the competition between exchange and magnetostatic energies modifies the stripe period and promotes the formation of new domain structures that are not observed in single-film stripes. Laterally modulated films are another interesting system in which the magnetic interactions play a major role in the characteristics of the stripe structure [8, 22]. These nanostructures are obtained by means of electron beam lithography, starting from a single continuous film, and they consist of periodic parallel bands of two different thicknesses, whose period and thickness are specifically chosen to study the competition between energy terms. Distinct regimes can be found in which the stripe structure in different bands can switch coherently or independently, in this last case forming stripes rotated by 90 degrees in each band.

The large difference in the stripe period of medium and low Q-value films can also be used to study the effects of magnetic interactions on the stripe structure in bilayers formed by two FM films. The individual layer thickness of this relatively simple structure can be manipulated easily to promote the appearance of the stripe structure in one or both layers. A detailed study of different sets of samples allowed us to follow the evolution of the magnetic domain configuration and characterize the influence of the magnetic interactions on the stripe period and the critical thickness.

2. Sample preparation and structural characterization

FePt/permalloy (Py) bilayers were fabricated by dc magnetron sputtering on naturally oxidized Si (1 0 0) single-crystal substrates. The samples were deposited from 3.8 cm diameter FePt and NiFe alloy targets with nominal atomic compositions of 50/50 and 80/20, respectively. The deposition conditions were: base pressure $< 1.5 \times 10^{-6}$ Torr, sputtering power 20 W, argon pressure 3 mTorr, and deposition rates $v_{Py} = 0.128(4)$ nm s^{-1} and $v_{FePt} = 0.204(4)$ nm s^{-1}. To prevent oxidation effects, all the samples were covered with ~2 nm of RF-sputtered SiO_2. We grew two different sets of samples: in series A the Py film was in contact with the substrate and FePt was deposited on top of the Py, while in series B FePt was grown first and Py was grown afterwards. Samples of series A are labeled Pyx/FePty, while series B samples are labeled FePty/Pyx (where x and y indicate the film thickness in nanometers). Furthermore, a set of Py single-layer films with thicknesses of 25 nm $\leqslant d \leqslant$ 360 nm was fabricated for control purposes. These films were grown with the same parameters used for the bilayers and were also capped with ~2 nm of SiO_2. For the FePt single films, we used the results published in [5, 25], in which the films were sputtered from the same FePt target using similar fabrication conditions. In table 1 we detail the individual nominal film thickness of each bilayer. In series A the Py thickness was kept fixed at $d_{Py} = 300$ nm and 10 nm $\leqslant d_{FePt} \leqslant 60$ nm (except for one sample in which both layers were 100 nm thick), while in series B $d_{FePt} = 100$ nm and 10 nm $\leqslant d_{Py} \leqslant 300$ nm. The thicknesses were chosen specifically to obtain a stripe structure in the fixed-thickness bottom layer, while covering a range around d_{cr} for the top layer. The total bilayer thickness was checked with a profilometer and, on average, was coincident with the nominal thickness to within a 6% margin.

Table 1. The individual film thickness of each bilayer in the two series. In A, the Py was in contact with the Si substrate, while in B the FePt was grown first. The thicknesses of the permalloy and FePt (from [5, 25]) in the control series are also given.

Series A		Series B		control	
Py	FePt	FePt	Py	Py	FePt
		d (nm)			
300	10	100	10	25	9
300	20	100	100	135	19
300	30	100	200	200	28
300	40	100	300	260	35
300	50			300	42
300	60			325	49
100	100			360	56

Structural characterization of the samples was performed using a PANalytical Empyrean x-ray diffractometer in a conventional Bragg–Brentano $\theta - 2\theta$ scan, in which 2θ is the angle between the incident and the diffracted beam. Diffractograms were obtained using Cu K_α radiation ($\lambda_{Cu} = 0.154\,18$ nm). Both FePt [31, 32] and permalloy [38] sputtered thin films tend to grow in the disordered fcc A1 crystalline phase and when they are sputtered on top of amorphous substrates a relatively strong [1 1 1] texture is generally found in the two alloys [31, 32, 39, 40]. In figure 1 we show selected diffractograms of samples Py100/FePt100 and Py300/FePt60 from series A, and samples FePt100/Py100 and FePt100/Py300 from series B. We can see that the most intense reflections correspond to the (1 1 1) planes, indicating a strong [1 1 1] texture normal to the film plane. We did not observe any systematic variation in the angular position of the (1 1 1) reflection of the FePt and

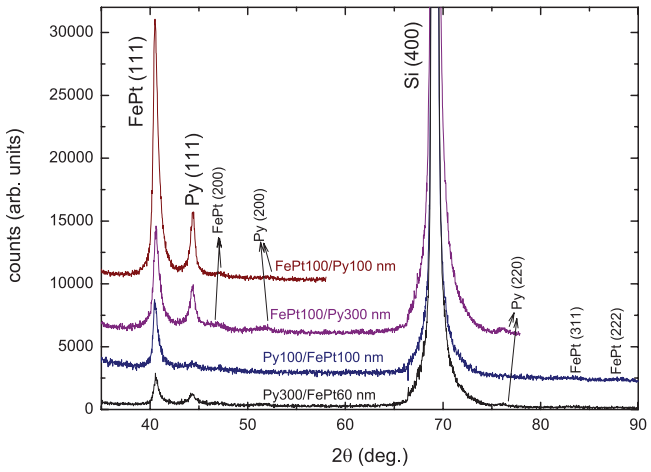

Figure 1. X-ray diffractograms for selected bilayers. The most intense reflections correspond to the (1 1 1) planes of Py and FePt. The strong Si (4 0 0) reflection corresponds to the substrate.

Py for different deposition ordering or film thickness. From the different diffractograms we calculated the average interplanar distances normal to the film plane, $d^{\mathrm{Py}}_{1\,1\,1} = 0.204(6)$ nm and $d^{\mathrm{FePt}}_{1\,1\,1} = 0.222(4)$ nm, and used these values to estimate the corresponding lattice parameters: $a_{\mathrm{Py}} = 0.353(10)$ nm and $a_{\mathrm{FePt}} = 0.385(7)$ nm. These estimates are in agreement with the lattice parameter measured in the control samples and the reported values for permalloy [41] ($a_{\mathrm{Py}} = 0.355$ nm) and FePt [31, 32] ($a_{\mathrm{FePt}} = 0.3833(5)$ nm). It must be kept in mind that residual stresses are always present in thin films, producing a strain that depends on the grain orientation [31]. Note that there is an $\sim 8\%$ mismatch between both lattices, which, in the range of thicknesses involved in this study, is large enough to prevent an elastic deformation of the top layer in order to match the lattice parameter of the bottom film. In the case of FePt films, the [1 1 1] texture is quite strong. From the diffractograms we estimated $I^{\mathrm{FePt}}_{(1\,1\,1)}/I^{\mathrm{FePt}}_{(2\,0\,0)} > 20$, while the intensity ratio for a collection of randomly oriented grains should be $I^{\mathrm{FePt}}_{(1\,1\,1)}/I^{\mathrm{FePt}}_{(2\,0\,0)} \sim 2$. Permalloy films seem to develop a less marked [1 1 1] texture, with an intensity ratio of $I^{\mathrm{Py}}_{(1\,1\,1)}/I^{\mathrm{Py}}_{(2\,0\,0)} \sim 10$, compared to $I^{\mathrm{Py}}_{(1\,1\,1)}/I^{\mathrm{Py}}_{(2\,0\,0)} \sim 1.8$ for the random case.

3. Magnetic measurements

Room temperature hysteresis loops were measured using a LakeShore model 7300 vibrating sample magnetometer (VSM) capable of a maximum field of 20 kOe. Magnetooptic Kerr effect measurements (MOKE) were performed in homemade equipment using a red laser ($\lambda = 632$ nm) with 1 mW power, vertical incident polarization and a longitudinal configuration. The magnetic field was applied parallel to the film plane, with a maximum value of 4 kOe. When studying metallic thin films, the MOKE technique probes the surface region determined by the skin depth, which is of the order of 10–20 nm in most metals [42]. This property is very useful because it can be used to separate the magnetic behavior of the bilayer, only analyzing the response of the top film. The surface magnetic domain structure of the films was studied by magnetic force microscopy with a Veeco Dimension 3100 AFM/MFM with Nanoscope IV electronics. We used medium moment, medium coercivity magnetic MESP tips from either Bruker or NT-MDT. As the tip was magnetized along its axis, the force gradient normal to the film plane was detected in all cases. To obtain the magnetic images we used the tapping lift mode with a second scan separation of ~30 nm and phase detection. Images were acquired in the remanent state (after externally saturating the samples in a 5 kOe field), or in an applied in-plane field generated by a homemade electromagnet that operates in the ±300 Oe range to minimize the rotation of the tip magnetization.

3.1. DC magnetization: vibrating sample magnetometer and the magnetooptic Kerr effect

The reported [5] critical thickness for the observation of stripe domains in FePt films grown in the same conditions as our samples is $d^{\mathrm{FePt}}_{\mathrm{cr}} \sim 32$ nm. For Py, the critical thickness is strongly dependent on the preparation conditions, with the reported values [34, 43–45] being in the range of 85–200 nm, but in all cases $d^{\mathrm{FePt}}_{\mathrm{cr}} < d^{\mathrm{Py}}_{\mathrm{cr}}$. The magnetic measurements in the Py control series showed a stripe domain structure for $d_{\mathrm{Py}} \geqslant 200$ nm. Fitting the stripe period λ^{Py}_s as a function of film thickness with a square-root law and extrapolating this behavior to the thickness, where [15] $d_{\mathrm{Py}} = \lambda^{\mathrm{Py}}_s/2$, we estimated $d^{\mathrm{Py}}_{\mathrm{cr}} = 185(15)$ nm. Apart from having different critical thicknesses, the Py and FePt thin films with stripe domains showed quite different coercivities ($H^{\mathrm{Py}}_{\mathrm{c}} \sim 20$ Oe and $H^{\mathrm{FePt}}_{\mathrm{c}} \sim 150$ Oe) and in-plane saturation fields for the alignment of the stripe structure ($H^{\mathrm{Py}}_s \sim 120$ Oe and $H^{\mathrm{FePt}}_s \sim 1200$ Oe). These two properties, together with the overall shape of the hysteresis loops, can be used to analyze the magnetic coupling between both layers. As an example, in figure 2(a) we show the individual hysteresis loops for Py300 and FePt100 samples measured in the VSM (both curves have been normalized by the film area, instead of the volume, to account for the different film thickness). If these two loops are added algebraically, we obtain the curve of figure 2(b), which is typical of a completely uncoupled system. Note the two-step behavior at $H^{\mathrm{Py}}_{\mathrm{c}}$ and $H^{\mathrm{FePt}}_{\mathrm{c}}$ associated with the inversion of the magnetization in each individual layer. The actual M versus H curve of the corresponding bilayer sample measured with the VSM is shown in figure 2(c). We can see that the loop shape of the bilayer is considerably different from that of figure 2(b), indicating a simultaneous reversal of both films, related to the presence of magnetic coupling. The effects of magnetic coupling on the loop shape as a function of the top FePt film thickness in series A (Py = 300 nm) are shown in figure 3. We present in parallel the same samples measured by VSM and MOKE (which only senses the top 10–20 nm) to stress the differences that appear when the top layer thickness varies. For $d_{\mathrm{FePt}} \leqslant d^{\mathrm{FePt}}_{\mathrm{cr}} \sim 30$ nm, the FePt layer magnetization follows the behavior of the bilayer closely, which is dominated by the bottom Py film (see figures 3(a)–(c)), while from $d_{\mathrm{FePt}} = 40$

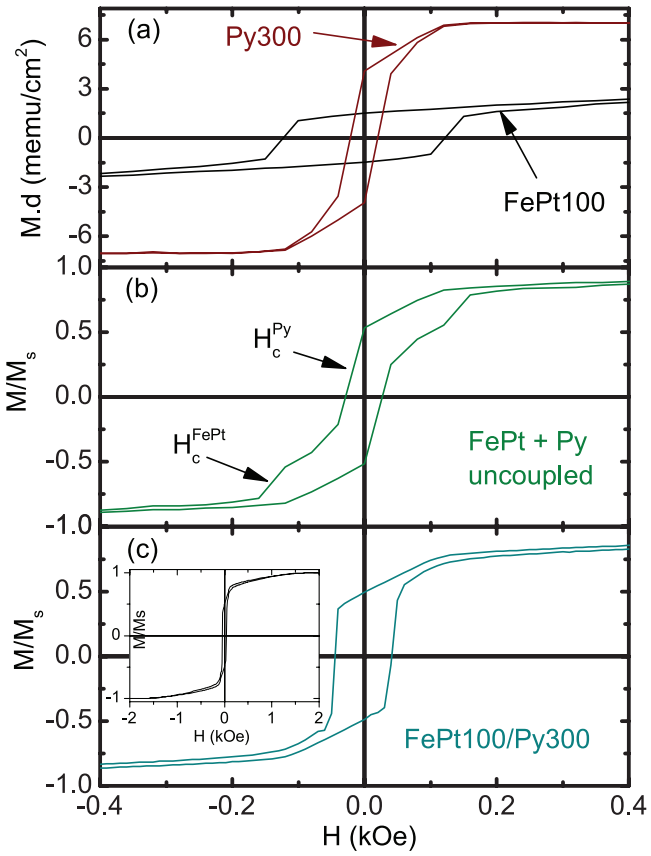

Figure 2. (a) Hysteresis loop for Py300 and FePt100 control films. The magnetization was multiplied by the film thickness to account for the different contribution of each layer. (b) Normalized numerical addition of the curves in (a). (c) Normalized hysteresis loop of the bilayer FePt100/Py300 measured with the VSM. The inset shows the same curve in an extended range, with $H > H_s^{\mathrm{FePt}}$.

nm the MOKE and VSM data start to show that there are two different saturation fields for the bottom and the top layers (figures 3(d)–(f)), which reach considerably different values for $d_{\mathrm{FePt}} = 50$ and 60 nm. On the other hand, the coercive field of the top film is very similar to that of the bilayer, indicating a simultaneous magnetization reversal. This result is somewhat unexpected and suggests that there is a change in the magnetic coupling mechanism of the bilayer when the top film thickness is above the critical value, $d_{\mathrm{cr}}^{\mathrm{FePt}}$.

In figure 4(a) we show the coercivities of the bilayers of series A as a function of the FePt thickness. It can be seen that approximately the same coercive field is found using the VSM and the MOKE techniques. Note, however, that the corresponding coercive field for a single FePt film in the region $d > d_{\mathrm{cr}}^{\mathrm{FePt}}$ is three–fives times larger than the one observed in the bilayer. This again is an indication of the different magnetic reversal mechanism of FePt when it is in contact with Py. In the case of the bilayers of series B a single-step magnetization versus field curve was also observed. The coercive field tends to be reduced when the Py thickness increases, as can be seen in figure 4(b). In addition, the coercive field of the top layer is coincident with that of the bilayer, except for in thinner Py films, where somewhat smaller values were found in the MOKE experiments. The coercivity of the reference Py film is much smaller than that of the bilayer for $d < d_{\mathrm{cr}}^{\mathrm{Py}}$ and converges to the bilayer values for thicker Py layers.

The exchange spring magnet (ESM) model [46] can be used as a simple approach to consider the effects of interlayer coupling in our bilayers. This model describes the effects of interlayer exchange interactions between soft and hard magnetic films, which are characterized by exchange stiffness A, anisotropy K, thickness d and domain wall thickness $\delta = \pi\sqrt{A/K}$. The model predicts that when the soft layer is thinner than a critical value, $d_s^{\mathrm{cr}} \sim \delta_h = \pi\sqrt{A_h/K_h}$ (δ_h is the domain wall thickness of the hard layer), it couples rigidly to the hard layer and the system rotates as a whole when a magnetic field is applied. In this situation we can estimate the average coercive field of the bilayer from the individual layer thicknesses and coercivities,

$$\langle H_{\mathrm{c}}\rangle \sim \frac{d_{\mathrm{FePt}} H_{\mathrm{c}}^{\mathrm{FePt}}(d_{\mathrm{FePt}}) + d_{\mathrm{Py}} H_{\mathrm{c}}^{\mathrm{Py}}(d_{\mathrm{Py}})}{d_{\mathrm{FePt}} + d_{\mathrm{Py}}}. \qquad (1)$$

The predicted coercivities from equation (1) are plotted as a dashed line in figures 4(a) and (b). The overall experimental behavior is in general well described in both series of bilayers, but discrepancies are observed in series B for $d_{\mathrm{Py}} > d_{\mathrm{cr}}^{\mathrm{Py}}$. Using the parameters for the FePt A1 phase [5], we estimated $d_s^{\mathrm{cr}} \sim 25$ nm, and so we did not expect a uniform reversal in most of the bilayers. It must be also remembered that this model applies when the hard layer is totally pinned and the reversal of the soft layer occurs by coherent rotation, which is not the case in the samples that present a stripe structure.

3.2. Magnetic force microscopy

We observed a stripe domain structure in all the studied samples, with the exception of control single Py films with $d_{\mathrm{Py}} \leqslant 135$ nm. Magnetic images acquired in the remanent state are shown in figure 5. In the bilayers of series A for $d_{\mathrm{FePt}} \lesssim 40$ nm the stripe structure is very similar to that of the Py300 reference sample, consisting of almost parallel stripes with very few bifurcations and a stripe half-period $\lambda_s/2 \sim 300$ nm that increases slowly with the FePt thickness, as can be seen in figure 6(a). For $d_{\mathrm{FePt}} > 40$ nm we found a double stripe structure that resembled 'fern leaves' composed of almost parallel domains (wavelength $\lambda_s/2 \sim 300$ nm), which could be associated with the Py layer, and more disordered stripes of shorter wavelength that were oriented at different angles, around $\pm 45°$ with respect to the vertical direction. The two different periods for $d_{\mathrm{FePt}} > 40$ nm were decomposed using the filtering option from the FFT tool of the WSxM package [47] and were also plotted in figure 6(a) with open symbols. The larger period stripe structure decreases its value, reaching approximately the period for a 300 nm single Py film. The FePt-like stripes show periods that are somewhat larger than those of the reference films of the same thickness. The nonparallel double-domain structure is a clear indication of an interaction between Py and FePt layers that overcomes the rotational anisotropy of the FePt film and prevents a parallel alignment of the two stripe

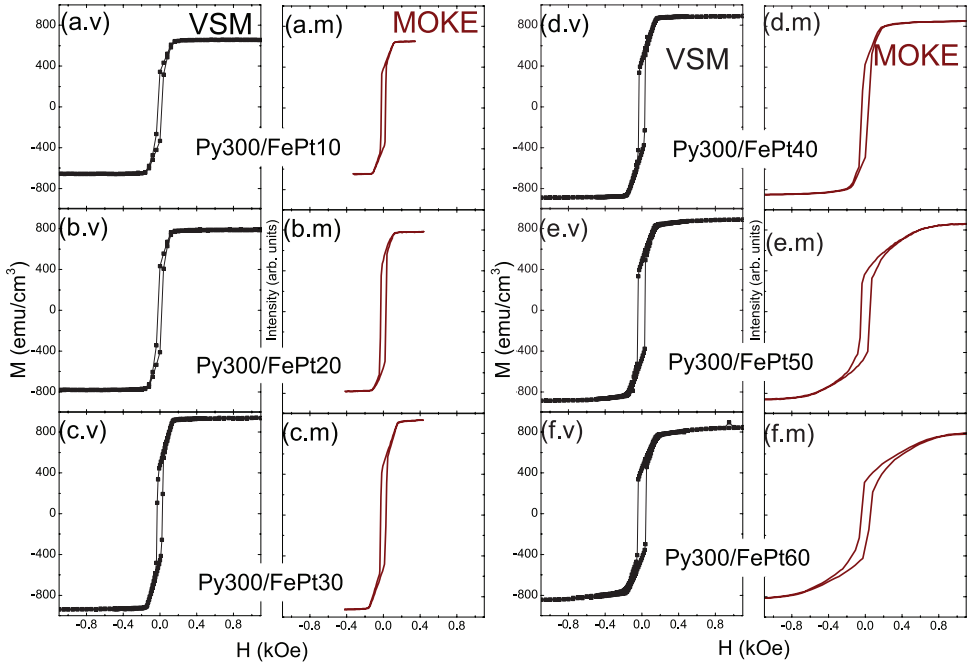

Figure 3. Hysteresis loops for the series A samples (Py300/FePtx), measured using VSM and the magnetooptic Kerr effect.

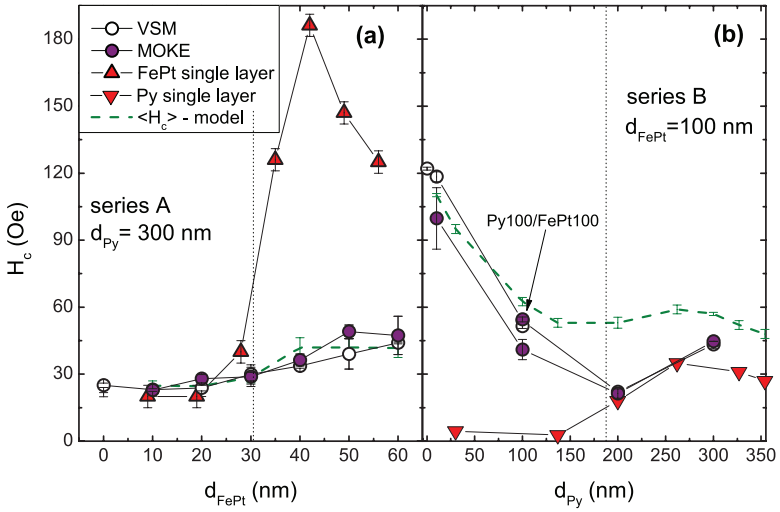

Figure 4. Coercive field as a function of (a) FePt film thickness for $d_{\mathrm{Py}} = 300$ nm (series A) and (b) Py layer thickness for $d_{\mathrm{FePt}} = 100$ nm (series B), as obtained from the VSM and the MOKE measurements. As a reference, we also show the coercivities of single FePt [5] and Py films. The dashed curves were obtained from equation (4). The vertical dotted lines separate the regions of planar and stripe domains for single films.

structures. For this series of samples we would have expected changes in the stripe structure starting from the bilayer Py300/FePt40, because $d_{\mathrm{cr}}^{\mathrm{FePt}} \sim 32$ nm. In figure 5 no clear evidence of a short period domain structure can be observed in the remanent state for this sample. However, we will show later that when a magnetic field is applied, a stripe domain structure related to FePt can be detected for fields above a critical value. The nonparallelism of the two stripe structures for $d_{\mathrm{FePt}} > 40$ nm can be explained if, in addition to the interlayer exchange interaction, we consider the dipolar stray field originated by the Py stripe structure. We should keep in mind that the structure of parallel domains generates stray fields perpendicular to the stripe direction. If we call x the in-plane coordinate perpendicular to the stripes and z the out-of-plane coordinate, it is possible to arrive at the following set of equations for the stray field in the case of strong stripe domains [37]:

$$H_x = 2M_\perp \ln\left[\frac{\cosh(2\pi z/\lambda_s) - \sin(2\pi x/\lambda_s)}{\cosh(2\pi z/\lambda_s) + \sin(2\pi x/\lambda_s)}\right], \qquad (2)$$
$$H_z = 4\pi M_\perp \arctan\left[\cos(2\pi x/\lambda_s)/\sinh(2\pi z/\lambda_s)\right].$$

The model assumes up and down domains with vanishingly small domain walls. It predicts a periodic variation of both components of the stray field in the x-axis. The stray fields obtained from equation (2) should be taken as an upper bound for the case of weak stripe domains, where closure domains tend to reduce the stray field. From the hysteresis loops of Py

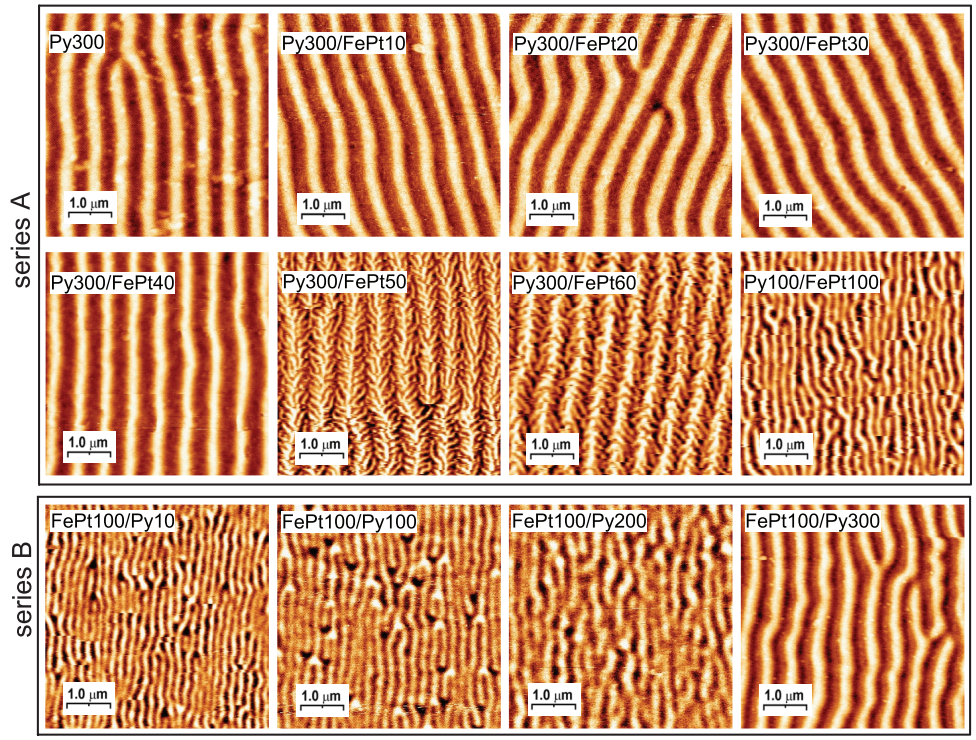

Figure 5. MFM images for series A and B samples and the Py300 control film, obtained at remanence after saturation in a field of 5 kOe. The image size is $5 \times 5\ \mu$m in all cases.

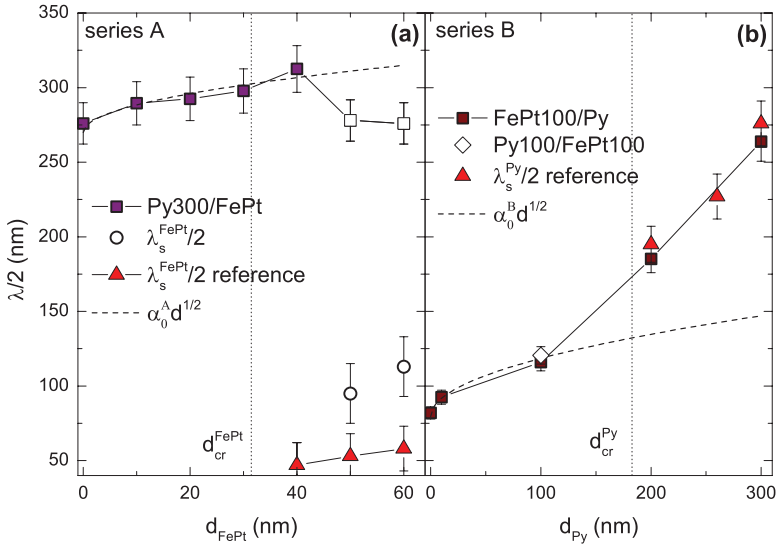

Figure 6. Stripe half-period of the series A and B bilayers obtained from MFM images (full squares). In (a) we plot the individual periods of the double-stripe structure with open symbols. We also show the reference stripe period from single FePt and Py films (triangles), with the corresponding critical thickness (dotted vertical lines). The dashed lines correspond to a square root dependence model of the stripe period with the total bilayer thickness.

films of 300 nm it is possible to estimate an upper bound for the perpendicular component of the magnetization, $M_\perp \sim 250$ emu cm^{-3}. Using equation (2) we estimated a maximum stray field of $H_x(z=0) \sim 5000$ Oe at the position of the domain wall and $H_x(z=0) = 0$ at the center of the stripe. For $z = 60$ nm the maximum field is reduced to $H_x(z = 60\ \text{nm}) \sim 300$ Oe. Even if we average the H_x component in a semiperiod we obtain $\langle H_x(z=0)\rangle \sim 1150$ Oe and $\langle H_x(z = 60\ \text{nm})\rangle \sim 190$ Oe. These stray field values are of the order of the rotational anisotropy of FePt [5] films, so that one could expect a partial rotation of the FePt stripes in the direction of H_x due to the dipolar interaction. In the case of the films of series B (lower panel of figure 5) stripe domains are observed for all the samples. For relatively thin Py layers the stripe period increases gradually with the Py thickness and for $d_{Py} > d_{cr}^{Py}$ a sharp increase is observed (see figure 6(b)), which is associated with the formation of a stripe structure in the Py layer. Note that even in the case of a 100 nm Py film ($d_{Py} < d_{cr}^{Py}$) covering a 100 nm FePt layer a stripe structure is observed, which indicates that in the remanent state the Py film tends to copy the FePt domain

structure. As can be seen in figure 6(b), the stripe period of this sample is almost identical to the reciprocal bilayer Py100/FePt100, evidencing the fact that the deposition order of the films does not influence the magnetism of the bilayer.

Figure 6 shows that the stripe half-period of both series of films presents a discontinuity at the critical thickness for the formation of stripe domains in the top layer. If we assume that in the low thickness region the bilayer responds as a unique film, the stripe period as a function of the bilayer thickness can be described using the Kooy [11] or Murayama [12] models, which predict a square root variation of the period with film thickness,

$$\frac{\lambda_s}{2} \simeq \alpha_0 \sqrt{d}. \tag{3}$$

Kooy's model describes the observed experimental behavior better [5], with a constant $\alpha_0 \sim \left[\frac{\pi^2\sqrt{AK_\perp}}{8M_s^2}\left(1+\sqrt{1+\frac{1}{Q}}\right)\right]^{1/2}$ that can be obtained from parameters that are already known. Using our own data ($M_s^{\mathrm{FePt}} = 1050$ emu cm^{-3}, $K_\perp^{\mathrm{FePt}} = 1.5\times10^6$ erg cm^{-3}, $M_s^{\mathrm{Py}} = 800$ emu cm^{-3}, $K_\perp^{\mathrm{Py}} = 0.14\times10^6$ erg cm^{-3}) and reported values for the A constant of FePt [4] and Py [48], we estimated $\alpha_0^{\mathrm{Py}} \sim 7(1)$ nm$^{1/2}$ and $\alpha_0^{\mathrm{FePt}} \sim 6(1)$ nm$^{1/2}$. By fitting the thickness dependence in figure 6 with a square root law (equation (3)), we obtained $\alpha_0^{\mathrm{A}} \sim 6(1)$ nm$^{1/2}$ for series A and $\alpha_0^{\mathrm{B}} \sim 3.9(7)$ nm$^{1/2}$ for series B. Although we had a relatively small number of samples for the fitting, it is clear that in both series of bilayers the stripe period increases when the total thickness is increased, suggesting that for $d < d_{\mathrm{cr}}$ the two films are coupled and behave as a single film. In a strongly coupled bilayer with varying film thicknesses, equation (3) must be applied with care because the α_0 value depends on the relative quantity of each component. For series A one would expect an α_0 parameter closer to the value of α_0^{Py} (because the bilayer is mostly made of Py), which is gradually reduced by the proportional contribution of α_0^{FePt}. For series B an α_0 closer to α_0^{FePt} is expected. We have indeed found that the experimentally obtained values are (within error) consistent with the predicted behavior. When applying theoretical models for single films it is important to consider that the thickness entering into equation (3) is not necessary equal to the bilayer thickness d if the magnetic coupling does not propagate to the whole volume.

At this point one might question the origin of the magnetic structure we are observing with the MFM. Is it coming from top film, from the added contribution of both films, or from the coupled bilayer as a whole? The question does not have a single easy answer, because it depends on the individual layer thickness and the interlayer coupling. As the MFM senses the stray fields above the film surface it is necessary to analyze how they are modified in the case of a magnetic bilayer. As a general rule, these stray fields from the magnetic domains extend a distance that is approximately equal to the domain size in the air above the surface [49, 50]. In the case of the bilayers of series A, the 300 nm Py film is covered with a ferromagnetic FePt film with a relative permeability much larger than 1. Using finite element analysis software, we estimate that a uniformly magnetized layer of 40 nm of FePt with the relative permeability obtained from the measured magnetization curve would reduce the vertical component of the permalloy stray field due to the stripe structure by a factor of more than 20. In the first five images of figure 5 there is no significant reduction of the MFM signal, which may be taken as an indication that the top FePt film is exchange coupled to the Py layer and tends to copy the underlying domain structure of the Py film. This is consistent with the VSM and MOKE hysteresis loops of figures 3(a)–(d), which indicate a similar magnetic behavior for the bilayer and the top FePt film, and also with the discussion concerning the increase in the stripe period with the total bilayer thickness. Similar findings were reported for YIG/Fe bilayers, where it was shown that a sufficiently thin Fe layer ($d < 20$ nm) deposited on top of a YIG film that displays stripe domains tends to copy the underlying magnetic structure. Thicker Fe films switch to an in-plane configuration, because the magnetostatic energy overcomes the interlayer exchange [51]. In our case, when $d_{\mathrm{FePt}} > 40$ nm, the FePt thickness is larger than $d_{\mathrm{cr}}^{\mathrm{FePt}}$, and this layer tends to form a second stripe structure. However, as already discussed, there is competition between the interlayer exchange and the dipolar stray field originated by the underlying Py stripe structure, which favors the orientation of the short period FePt-like stripe structure at an angle of $\sim 45°$.

The interlayer magnetic coupling in the bilayers with a double stripe structure is also tested by acquiring MFM images with applied magnetic field. The idea of this study is to determine the field dependence of the two stripe structures. To obtain the images, we apply the maximum available field in the negative direction, set the field to zero, and then apply positive fields that are changed manually in discrete steps every 100 scan lines. In figure 7 we show the MFM data for the three series A films with $d \geqslant 40$ nm. In the Py300/FePt40 sample no significant changes occur at relatively low fields. For $H > 160$ Oe the Py-like stripe structure disappears and a faint low-period disordered stripe structure can be observed. Note that this structure cannot be detected in the remanent state and it only becomes visible when the bottom Py film is completely aligned in the film plane. A similar behavior is found in the Py300/FePt50 and Py300/FePt60 bilayers, but in these samples a somewhat larger field is required to saturate the Py-like stripes, $H_s^{\mathrm{Py}} \lesssim 200$ Oe. The short period stripes, which at low applied fields are at $\sim$45° to the Py-like stripes, gradually align to the direction of H for $H > H_s^{\mathrm{Py}}$. Note also that in the low field region (20 Oe $< H <$ 50 Oe, coincident with the coercive field of the bilayer) there is a rotation of the short period stripes by approximately 90°. Analyzing this behavior, it is possible to understand the VSM and MOKE results shown in figure 8 (and sketched in the inset) better. In the remanent state the Py-like stripe structure remains parallel to the direction of the last applied field due to the rotational anisotropy. The short period FePt-like stripes are not parallel to the underlying stripe structure because of the presence of a perpendicular component of the dipolar magnetic field. When the coercive field of the bilayer (H_c) is reached, the in-plane magnetization of the Py-like structure rotates by 180°, but the perpendicular component remains unaltered.

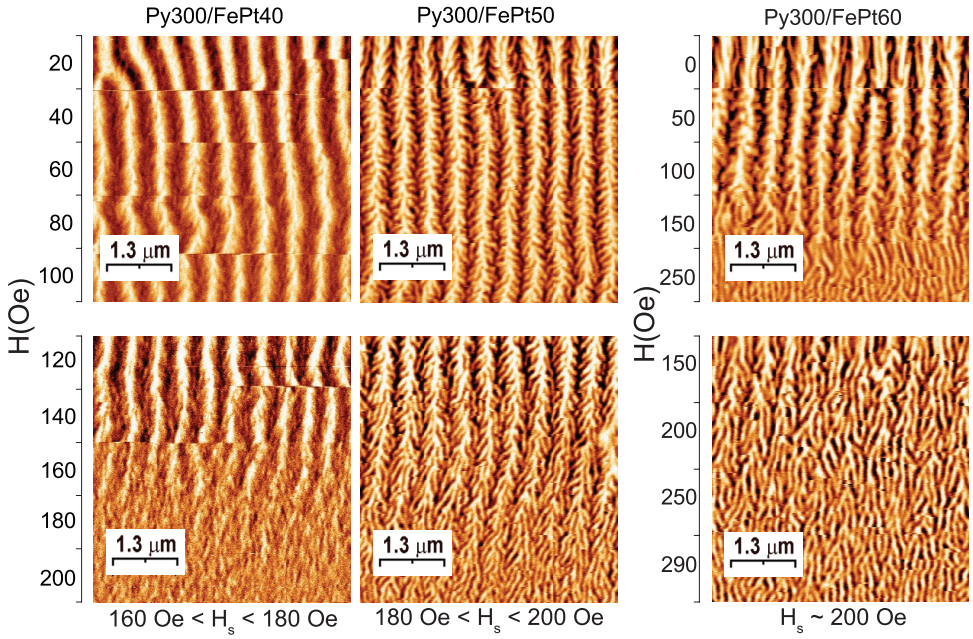

Figure 7. MFM images of the series A samples ($d_{Pt} \geqslant 40$ nm) for different applied magnetic fields. We indicate the approximate field where the Py-like stripe structure is no longer observed with H_s. The coercive fields are $H_c = 34, 39$ and 44 Oe for FePt of 40, 50 and 60 nm, respectively.

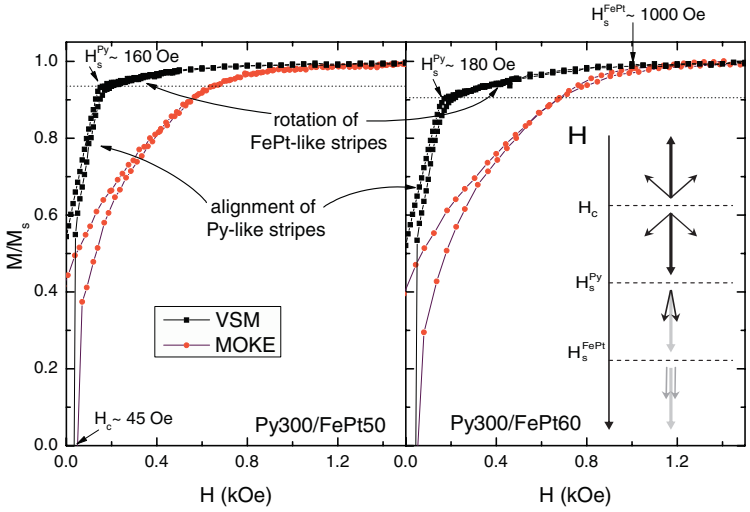

Figure 8. First quadrant of the hysteresis loops of Py100/FePt50 and Py100/FePt60 measured using the VSM and MOKE techniques. We indicate the in-plane saturation field for the Py-like and FePt-like stripes. The inset is a toy model of the field dependence of the in-plane magnetization direction of the Py (large arrow) and FePt (smaller arrows) layers. The black/gray indicates the presence/absence of an out-of-plane component.

This reversal is accompanied by a rotation of the in-plane magnetization of the FePt layer. Note that the VSM and MOKE curves have almost the same coercivity for both bilayers. Increasing the applied field produces the in-plane alignment of the bottom layer (indicated with a gray arrow in the sketch) and the gradual rotation of the short period stripes to the direction of the magnetic field at H_s^{Py}, coincident with the values found from the MFM images with applied field (see figure 7). If the magnetic field is further increased, the magnetization of both layers finally aligns parallel to H with a zero out-of-plane component (gray arrows in figure 8).

We also test the effects of rotational anisotropy on the interaction between the two stripe structures by applying the magnetic field perpendicular to the initial direction of the stripes. We make these measurements using vectorial VSM (which can measure the magnetization component parallel and perpendicular to the applied field) and MFM. In figure 9(a) we show the magnetization curves for the Py300/FePt50 sample obtained after saturating the bilayer in a field of 5 kOe in the y-axis, setting the field to zero, rotating the sample by 90°, and measuring both components of the magnetization. It is observed that M_y decreases relatively slowly until $H \sim 40$ Oe, and then a fast reduction occurs.

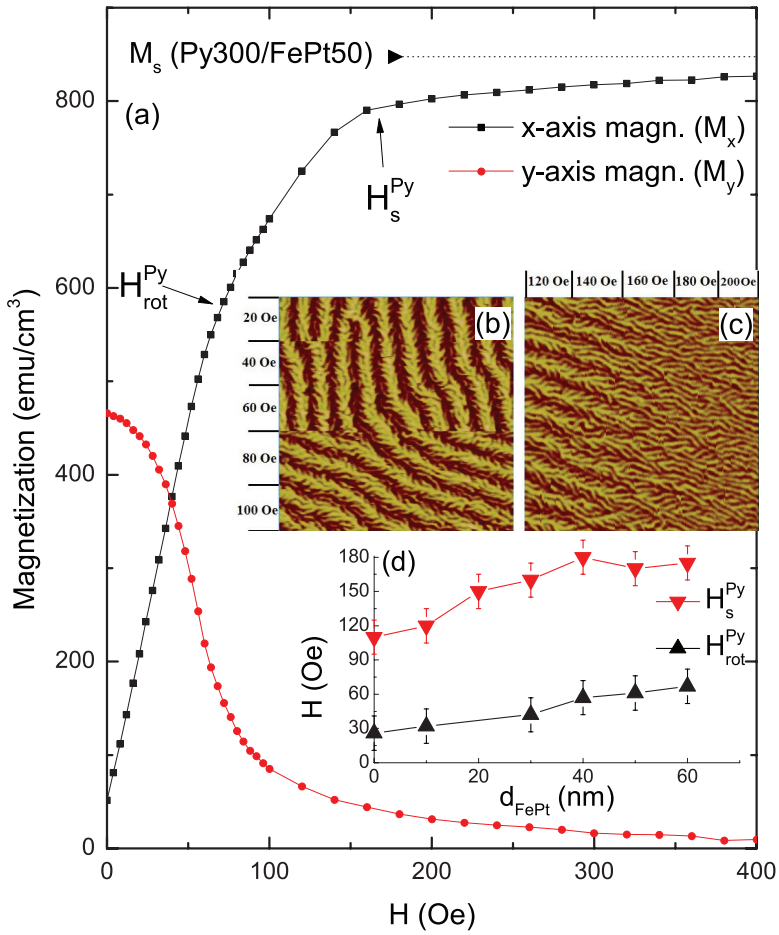

Figure 9. (a) First quadrant of the hysteresis loops of Py100/FePt50 measured with vectorial VSM. The sample was saturated in the *y*-axis, rotated 90°, and measured with the field applied in the *x*-axis. The MFM images were acquired following the same protocol. (b) and (c) $5 \times 5\,\mu$m scans, with the fast scan axis in the horizontal and vertical directions, respectively. The magnetic field was changed after every 100 scan lines.

M_x increases almost linearly until the rotational field of the permalloy layer $H_{\rm rot}^{\rm Py} \sim 60$ Oe is reached (as can be seen in figure 9(b)), where it changes the slope and continues to increase approximately linearly until $H_{\rm s}^{\rm Py} \sim 160$ Oe. Note that complete magnetic saturation of the bilayer occurs for fields of the order of 1000 Oe. These results indicate that part of the principal stripe structure remains parallel to the initial direction, while a component of M, which is not aligned with H, rotates to the field direction. Similar results were recently reported for $Fe_{80}Ga_{20}$ thin films [7], and were attributed to the reorientation of the closure domains in the direction of the applied field. The linear variation of M_x may be interpreted as a rotation of the magnetization vector away from an easy axis defined by the stripe direction. As seen in figure 9(b), the double stripe structure seems to rotate rigidly towards the magnetic field direction for $H \gtrsim 60$ Oe, more-or-less coincident with the sharp decrease in M_y observed in figure 9(a). The permalloy magnetization aligns in-plane with the external field, causing the disappearance of the Py-like stripes for $H_{\rm s}^{\rm Py} > 160$ Oe, and only the short period stripes are left (see figure 9(c)), coincident with the field, where a change in slope is seen in figure 9(a). We make the same VSM measurements for the rest of the series A films and observe a smooth increase of $H_{\rm rot}^{\rm Py}$ and $H_{\rm s}^{\rm Py}$ (figure 9(d)) with the FePt thickness, again indicating that the interlayer interaction modifies the domain configuration and the magnetic anisotropy constants.

4. Conclusions

Analyzing two different sets of magnetic bilayers composed of films that can present stripe magnetic domains of different characteristics, we show that dipolar and exchange-like magnetic interactions must be considered in order to explain the observed magnetic behavior. When the top magnetic layer is thin enough, the bilayer essentially responds as a single film with average magnetic parameters. However, when both layers are thicker than their critical thickness, a complex double stripe structure is observed, caused mostly by dipolar interactions. The ability to control the geometry and periodicity of this peculiar stripe structure would open up the possibility of using it to obtain new functionalities in magnetic films for applications in spintronic and magnonic devices.

Acknowledgments

This work was supported in part by Conicet under grant no. PIP 112-201101-00482, by ANPCyT under grant no. PICT 2013-0401 and by U N Cuyo under grant no. 06/C421, all from Argentina. Technical support from Rubén E Benavides, César Pérez and Matías Guillén is gratefully acknowledged.

References

[1] Saito N, Fujiwara H and Sugita Y 1964 *J. Phys. Soc. Japan* **19** 421
[2] Hehn M, Padovani S, Ounadjela K and Bucher J P 1996 *Phys. Rev.* B **54** 3428
[3] Gehanno V, Hoffmann R, Samson Y, Marty A and Auffret S 1999 *Eur. Phys. J.* B **10** 457
[4] Okamoto S, Kikuchi N, Kitakami O, Miyazaki T, Shimada Y and Fukamichi K 2002 *Phys. Rev.* B **66** 024413
[5] Sallica Leva E, Valente R C, Martínez Tabares F, Vásquez Mansilla M, Roshdestwensky S and Butera A 2010 *Phys. Rev.* B **82** 144410
[6] Barturen M *et al* 2012 *Appl. Phys. Lett.* **101** 092404
[7] Fin S *et al* 2015 *Phys. Rev.* B **92** 224411
[8] Hierro-Rodríguez A, Cid R, Vélez M, Rodríguez-Rodríguez G, Martín J I, Álvarez-Prado L M and Alameda J M 2012 *Phys. Rev. Lett.* **109** 117202
[9] Belliard L, Kottler V, Mathet V, Chappert C and Valet T 1997 *J. Appl. Phys.* **81** 5315
[10] Bručas R, Hafermann H, Soroka I L, Iuşan D, Sanyal B, Katsnelson M I, Eriksson O and Hjörvarsson B 2008 *Phys. Rev.* B **78** 024421
[11] Kooy C and Enz U 1960 *Philips Res. Rep.* **15** 7
[12] Murayama Y 1966 *J. Phys. Soc. Japan* **21** 2253
[13] Sukstanskii A L and Primak K I 1997 *J. Magn. Magn. Mater.* **169** 31
[14] Bručas R, Hafermann H, Katsnelson M I, Soroka I L, Eriksson O and Hjörvarsson B 2004 *Phys. Rev.* B **69** 064411
[15] Hubert A and Schäfer R 2009 *Magnetic Domains* (Berlin: Springer)
[16] Labrune M and Carbucicchio M 2004 *J. Magn. Magn. Mater.* **269** 203
[17] Ebels U, Buda L D, Ounadjela K and Wigen P E 2002 *Spin Dynamics in Confined Magnetic Structures* I ed B Hillebrands and K Ounadjela (Berlin: Springer) ch 6, pp 167–217
[18] Utsumiya K, Seki T and Takanashi K 2011 *J. Appl. Phys.* **110** 103911
[19] Dastagir T, Xu W, Sinha S, Wu H, Cao Y and Yu H 2010 *Appl. Phys. Lett.* **97** 162506
[20] Wei J, Zhu Z, Feng H, Du J, Liu Q and Wang J 2015 *J. Phys. D: Appl. Phys.* **48** 465001
[21] Donzelli O, Bassani M, Spizzo F and Palmeri D 2008 *J. Magn. Magn. Mater.* **320** e261
[22] Hierro-Rodríguez A, Vélez M, Morales R, Soriano N, Rodríguez-Rodríguez G, Álvarez-Prado L M, Martín J I and Alameda J M 2013 *Phys. Rev.* B **88** 174411
[23] Samson Y, Marty A, Hoffmann R, Hehanno V and Gilles B 1999 *J. Appl. Phys.* **85** 4604
[24] Vásquez Mansilla M, Gómez J and Butera A 2008 *IEEE Trans. Magn.* **44** 2883
[25] Vásquez Mansilla M, Gómez J, Sallica Leva E, Castillo Gamarra F, Asenjo Barahona A and Butera A 2009 *J. Magn. Magn. Mater.* **321** 2941
[26] Burgos E, Sallica Leva E, Gómez J, Martínez Tabares F, Vásquez Mansilla M and Butera A 2011 *Phys. Rev.* B **83** 174417
[27] Jacobi D M, Sallica Leva E, Álvarez N, Vásquez Mansilla M, Gómez J and Butera A 2012 *J. Appl. Phys.* **111** 033911
[28] Guzmán J M, Álvarez N, Salva H R, Vásquez Mansilla M, Gómez J and Butera A 2013 *J. Magn. Magn. Mater.* **347** 61
[29] Álvarez N, Alejandro G, Gómez J, Goovaerts E and Butera A 2013 *J. Phys. D: Appl. Phys.* **46** 505001
[30] Álvarez N, Sallica Leva E, Valente R C, Vásquez Mansilla M, Gómez J, Milano J and Butera A 2014 *J. Appl. Phys.* **115** 083907
[31] Álvarez N R, Gómez J E, Moya Riffo A E, Vicente Álvarez M A, Vázquez Montalbetti M E, Goovaerts E and Butera A 2015 *J. Phys. D: Appl. Phys.* **48** 405003
[32] Álvarez N R, Gómez J E, Moya Riffo A E, Vicente Álvarez M A and Butera A 2016 *J. Appl. Phys.* **119** 083906
[33] Ben Youssef J, Vukadinovic N, Billet D and Labrune M 2004 *Phys. Rev.* B **69** 174402
[34] Ramos C A, Vassallo Brigneti E, Gómez J and Butera A 2009 *Physica* B **404** 2784
[35] Craus C B, Chezan A R, Siekman M H, Lodder J C, Boerma D O and Niesen L 2002 *J. Magn. Magn. Mater.* **240** 423
[36] Janicka K, Burtom J D and Tsymbal E Y 2007 *J. Appl. Phys.* **101** 113921
[37] Kiselev N S, Dragunov I E, Neu V, Röß ler U K and Bogdanov A N 2008 *J. Appl. Phys.* **103** 043907
[38] Coey J M D 2010 *Magnetism and Magnetic Materials* (New York: Cambridge University Press) p 387
[39] Parker M A, Hylton T L, Coffey K R and Howard J K 1994 *J. Appl. Phys.* **75** 6382
[40] Rozenberg E, Pelleg J, Dariel M P, Ezersky V, Mogilyanski D, Sariel J and Sade G 1997 *J. Magn. Magn. Mater.* **165** 342
[41] Snoeck E, Sinclair R, Parker M A, Hylton T L, Coffey K R, Howard J K, Lessmann A and Bienenstock A I 1995 *J. Magn. Magn. Mater.* **151** 24
[42] Bland J A C, Padgett M J, Butcher R J and Bett N 1989 *J. Phys. E: Sci. Instrum.* **22** 308
[43] Amos N, Fernandez R, Ikkawi R, Lee B, Lavrenov A, Krichevsky A, Litvinov D and Khizroev S 2008 *J. Appl. Phys.* **103** 07E732
[44] Wang G, Dong C, Wang W, Wang Z, Chai G, Jiang C and Xue D 2012 *J. Appl. Phys.* **112** 093907
[45] Soh W T, Phuoc N N, Tan C Y and Ong C K 2013 *J. Appl. Phys.* **114** 053908
[46] Fullerton E, Jiang J S and Bader S D 1999 *J. Magn. Magn. Mater.* **200** 392–404
[47] Horcas I, Fernández R, Gómez-Rodriguez J M, Colchero J, Gómez-Herrero J and Baro A M 2007 *Rev. Sci. Instrum.* **78** 013705
[48] Kim S D, Lee J J, Kim K H, Lim S H and Kim H J 1999 *IEEE Trans. Magn.* **35** 3397–9
[49] Szmaja W 2006 Recent Developments in the imaging of magnetic domains *Adv. Imaging Electron Phys.* **141** 175–256
[50] Szmaja W, Grobelny J and Cichomski M 2004 *Appl. Phys. Lett.* **85** 2878
[51] Chun Y S and Krishnan K M 2004 *J. Appl. Phys.* **95** 6858